

Pinching-Antenna System-Assisted Localization: A Stochastic Geometry Perspective

Jiajun He, *Member, IEEE*, Xidong Mu, *Member, IEEE*, Hien Quoc Ngo, *Fellow, IEEE*, and Michail Matthaiou, *Fellow, IEEE*

Abstract—This paper proposes a novel localization framework underpinned by a pinching-antenna (PA) system, in which the target location is estimated using received signal strength (RSS) measurements obtained from downlink signals transmitted by the PAs. To develop a comprehensive analytical framework, we employ stochastic geometry to model the spatial distribution of the PAs, enabling tractable and insightful network-level performance analysis. Closed-form expressions for target localizability and the Cramér–Rao lower bound (CRLB) distribution are analytically derived, enabling the evaluation of the fundamental limits of PA-assisted localization systems without extensive simulations. Furthermore, the proposed framework provides practical guidance for selecting the optimal waveguide number to maximize localization performance. Numerical results also highlight the superiority of the PA-assisted approach over conventional fixed-antenna systems in terms of the CRLB.

Index Terms—Cramér–Rao lower bound, localization, pinching antenna, received signal strength.

I. INTRODUCTION

PINCHING-antenna (PA) systems have garnered significant attention in recent years due to their reconfigurability and practical deployment potential [1]. Compared to traditional multiple-antenna systems, a PA system comprises multiple discrete dielectric particles, referred to as PAs, that are pinched on dielectric waveguides to facilitate signal transmission. Equally importantly, DOCOMO demonstrated in [2] that a PA system can be implemented in a cost-effective manner. Motivated by these promising characteristics, PA systems have been extensively studied in the literature to enhance communication functionality. The fundamental performance limits of PA systems under various network configurations were thoroughly examined in [3], demonstrating that a PA system can achieve significant performance gains over conventional antenna systems. In addition, a distinguishing feature of PA systems is the reconfigurability of the PAs. By adjusting their positions along the waveguide, the system can simultaneously serve multiple mobile users and enhance communication performance by minimizing the distance between each user and its associated PA.

Due to the advantages of PA systems, recent studies have investigated their potential to improve localization performance. For instance, Ding [4] analyzed the fundamental limits of a PA-assisted time-of-arrival (ToA) localization system in terms of the Cramér–Rao lower bound (CRLB), demonstrating that the use of PAs can significantly reduce localization error. Khalili *et al.* [5] investigated the large-scale deployment of waveguides to improve target diversity and sensing performance. Qin *et al.* [6] investigated how a PA system can be

used to enhance the performance of integrated sensing and communication (ISAC) systems in terms of communication and sensing rates, whereas the inner and outer bounds of the achievable communication–sensing rate region were derived in [7] to gain insights into the information-theoretic limits of PA-assisted ISAC systems. Although PA systems have demonstrated strong potential in enhancing sensing and localization performance, a significant challenge cannot be overlooked when applying them to target localization. The sparse deployment of PAs along dielectric waveguides may limit their ability to capture a wide range of signals transmitted by mobile users. The signal reception on a single waveguide equipped with multiple PAs can lead to significant inter-antenna coupling, which lowers the localization accuracy. To address this issue, prior works, such as [8] and [9], have proposed the usage of additional antenna arrays or leaky coaxial cables (LCCs) to capture echo signals reflected by the target for channel estimation and target localization.

From a practical implementation perspective, this work considers received signal strength (RSS)-based localization within a PA system, where multiple PAs transmit downlink signals to the target for localization.¹ In addition, to the best of our knowledge, existing studies on PA system-assisted localization primarily focus on system-level or link-level designs and fail to provide insights into how different system configurations affect the overall localization performance. Motivated by this limitation, we aim to develop a stochastic geometric framework that studies the impact of the spatial distribution of PAs on the localization performance, thereby enabling network-level performance analysis and system optimization. The main contributions of this paper are listed as follows:

- 1) *Stochastic Modeling of the PA System*: A unified evaluation framework is developed using stochastic geometry, providing valuable insights into the design of PA-assisted localization systems from a network-level perspective. To our knowledge, this is the first work to leverage the Poisson line process (PLP) for analyzing the localization performance of PA systems.
- 2) *Localizability and CRLB*: To assess whether the mobile user (target) can be localized with a sufficient signal-to-interference-plus-noise ratio (SINR), the target localizability is investigated. Tractable expressions for the

¹Different from ToA- and angle-of-arrival (AoA)-based localization, which typically require wideband signals or antenna arrays to obtain range and angle measurements, RSS-based localization offers a lower-complexity alternative by eliminating the need for such hardware and reducing the burden of acquiring location-dependent features [10].

CRLB and its distribution are then derived, offering valuable insights into how network configurations and channel characteristics influence the localization performance.

3) *Guideline for System Design*: A comprehensive evaluation is conducted to gain insights into the fundamental limits of PA-assisted localization. Numerical results show that the PA-assisted system achieves significantly improved localization accuracy compared to that of using uniform linear arrays (ULAs). In addition, the proposed stochastic geometric framework offers practical guidelines for optimizing the number of waveguides and configuring network parameters to meet the desired localization requirements.

II. SYSTEM MODEL

We consider a localization problem (see 1) in a two-dimensional (2D) space, where multiple PAs on waveguides transmit downlink signals to a target user for localization.

A. Network Model

According to Slivnyak's theorem [11], we assume that the target $\mathbf{p}_t = [x_t \ y_t]^T$ is located at the origin O , while the waveguides are randomly distributed within a 2D disk with center point at the origin and radius R_a according to a PLP with line density λ_l . Specifically, the k -th waveguide is modeled by an undirected line L_k , which is: $L_k(\rho_k, \theta_k) = \{(x, y) \in \mathbb{R}^2 : x \cos \theta_k + y \sin \theta_k = \rho_k\}$, where ρ_k denotes the perpendicular distance from the origin O to the k -th waveguide, while θ_k is its inclination angle. During localization, the m -th PA on waveguide k is activated from the predefined locations ($\mathbf{p}_{k,m} = [x_{k,m} \ y_{k,m}]^T$, where $k = 1, 2, \dots$ and $m = 0, 1, \dots$), while the predefined locations on the waveguide are modeled by a one-dimensional (1-D) homogeneous Poisson point process (HPPP) with node density λ_s . By indexing the waveguides in ascending order of their perpendicular distance ρ_k from the target, the probability density function (PDF) and cumulative distribution function (CDF) of the distance ρ_k to the k -th nearest waveguide are [12]

$$f_{\rho_k}(x) = \frac{e^{-2\pi\lambda_l x} (2\pi\lambda_l x)^k}{x(k-1)!},$$

$$F_{\rho_k}(x) = 1 - e^{-2\pi\lambda_l x} \sum_{n=0}^{k-1} \frac{(2\pi\lambda_l x)^n}{n!}. \quad (1)$$

Let $d_{k,1} = \|\mathbf{p}_{k,1} - \mathbf{p}_t\|$, where $\|\cdot\|$ denotes the Euclidean norm, be the distance between the target and the nearest PA ($m = 1$) on the k -th waveguide. Then, conditioned on ρ_k , the PDF and CDF of $d_{k,1}$ are, respectively, given by

$$f_{d_{k,1}|\rho_k}(r) = \frac{2\lambda_s r}{\sqrt{r^2 - \rho_k^2}} e^{-2\lambda_s \sqrt{r^2 - \rho_k^2}}, \quad (2)$$

$$F_{d_{k,1}|\rho_k}(r) = 1 - e^{-2\lambda_s \sqrt{r^2 - \rho_k^2}}.$$

B. Signal Model

Each waveguide activates its nearest PA to the target user, denoted as $\mathbf{p}_{k,1}$, during the localization process. Although all PAs serve the same target user for localization, the RSS sample has to be extracted from a specific PA to obtain distance

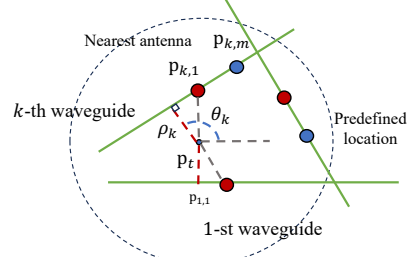


Fig. 1. Illustration of the PLP-based PA-assisted localization system.

information [10], [13]. Consequently, each PA on a different waveguide transmits different symbols, which introduces interference and compromises the localization performance. For example, in cellular networks, the base station (BS) transmits signals containing various types of information, such as the cell-ID, that enable mobile users to extract location information from the corresponding BS [13]. Thus, the signal received at the target user is

$$y = \sum_{k=1} \sqrt{P_t} h_{k,1} s_k + w_n, \quad (3)$$

where P_t is the transmit power at each PA, while s_k , where $\mathbb{E}\{|s_k|^2\} = 1$, is the symbol transmitted by the k -th waveguide, and $\mathbb{E}\{\cdot\}$ is the expectation operation; $h_{k,1}$ is the channel gain between the target and its nearest PA on the k -th waveguide, which is given by [3]

$$h_{k,1} = \frac{\sqrt{\eta} e^{-2\pi j \left(\frac{1}{\lambda} \|\mathbf{p}_t - \mathbf{p}_{k,1}\| + \frac{1}{\lambda_g} \|\mathbf{p}_{k,0} - \mathbf{p}_{k,1}\| \right)}}{\|\mathbf{p}_t - \mathbf{p}_{k,1}\|^{\alpha/2}}, \quad (4)$$

where $\eta = c^2/16\pi^2 f_c^2$, c is the speed of light, f_c is the carrier frequency, while λ and λ_g are the carrier and waveguide wavelength, respectively. Also, w_n is the additive white Gaussian noise (AWGN) with variance σ^2 , while α is the path-loss exponent. From (3) and (4), the SINR at the target associated with its nearest PA on the k -th waveguide is

$$\text{SINR}_k^{\text{PA}} = \frac{P_t |h_{k,1}|^2}{\sum_{i=1, i \neq k} P_t |h_{i,1}|^2}$$

$$= \frac{\eta P_t d_{k,1}^{-\alpha}}{\underbrace{\sum_{i=1, i \neq k} \eta P_t d_{i,1}^{-\alpha}}_{\text{interference from remaining PAs}} + \sigma^2} = \frac{d_{k,1}^{-\alpha}}{I + \sigma_n^2},$$

where $I = \sum_{i=1, i \neq k} d_{i,1}^{-\alpha}$, while $\sigma_n^2 = \frac{\sigma^2}{P_t \eta}$ is the normalized noise power. Since a line-of-sight (LoS) path between the target and the PA can be achieved by adjusting the PA location, the path-loss exponent typically ranges from 2 to 2.8 [13].

C. RSS Measurements

Considering a practical implementation of the PA-assisted localization system, the RSS-based scheme is considered. By assuming that the nearest predefined location on each waveguide has been determined, the RSS measured by the target user associated with the activated PA on the k -th waveguide is [10], [13]

$$r_{\text{RSS},k,1} = \ln P_{r,k,1} - \ln \eta - \ln P_t = -\alpha \ln d_{k,1} + n_p, \quad (5)$$

where $P_{r,k,1}$ is the received signal power at the target user transmitted by the activated PA on the waveguide k , while n_p is Gaussian distributed with variance $\sigma_p^2 = \frac{\ln 10}{10\alpha \mathbb{E}\{\text{SINR}_k^{\text{PA}}\}}$. Note that the value of α is normally obtained through field testing and calibration campaigns [10]. By collecting sufficient RSS measurements, the location estimate can be obtained using maximum likelihood estimation (MLE) as described in [10].

III. PERFORMANCE ANALYSIS

A. Target Localizability

To determine the target localizability, we evaluate the probability of detecting *at least* K waveguides during localization. Since the successful reception from the activated PA on the K -th nearest waveguide implies that all nearer waveguides are within the detection range, we investigate the probability that the SINR between the target and the selected PA on the K -th nearest waveguide exceeds a given threshold τ , given by

$$P(\text{SINR}_K^{\text{PA}} > \tau) = P\left(\frac{\eta P_t d_{K,1}^{-\alpha}}{\sum_{i=1, i \neq K} \eta P_t d_{i,1}^{-\alpha} + \sigma^2} > \tau\right). \quad (6)$$

To derive a closed-form expression of (6), the dominant interference analysis is adopted [14, Assumption 1]. Specifically, all interferers, except for the PA located on the nearest waveguide to the target, are approximated by their mean values. Then, we have the following proposition.

Proposition 1. *Considering a PA system with multiple waveguides, where the nearest predefined location to the target is activated to transmit downlink signals for localization, the probability of detecting at least K waveguides is*

$$\begin{aligned} & P(\text{SINR}_K^{\text{PA}} > \tau | d_{1,1}, d_{K,1}, \rho_K) \\ & \approx \int_0^{R_a} \int_0^{d_K} F_{d_{K,1} | \rho_K} \left(\left[\tau (\mathbb{E}\{I\} + \sigma_n^2) \right]^{-\frac{1}{\alpha}} \right) \quad (7) \\ & \quad \times f_{d_{1,1}}(r) f_{d_{K,1} | \rho_K}(x) f_{\rho_K}(y) dr dx dy, \end{aligned}$$

where $f_{d_{1,1}}(\cdot)$, $f_{d_{K,1} | \rho_K}(\cdot)$, $F_{d_{K,1} | \rho_K}(\cdot)$, and $f_{\rho_K}(\cdot)$ are provided in (1) and (2). Conditioned on the distances $d_{1,1}$, $d_{K,1}$, ρ_K , the interference I can be approximated by

$$\begin{aligned} & \mathbb{E}\{I_K | d_{1,1}, d_{K,1}, \rho_1, \rho_K\} \\ & \approx \begin{cases} d_{1,1}^{-\alpha} + \frac{2(K-2)}{2-\alpha} \frac{\rho_K^{2-\alpha} - \rho_1^{2-\alpha}}{\rho_K^2 - \rho_1^2} + \frac{2\pi\lambda_l}{\alpha-2} \rho_K^{2-\alpha}, & \alpha > 2, \\ d_{1,1}^{-2} + \frac{2(K-2)}{\rho_K^2 - \rho_1^2} \ln \frac{\rho_K}{\rho_1} + 2\pi\lambda_l \ln \frac{R_a}{\rho_K}, & \alpha = 2. \end{cases} \quad (8) \end{aligned}$$

Proof. See Appendix I. \square

For RSS-based localization, at least three waveguides are required to localize the target position without ambiguity [10]. **Proposition 1** characterizes the probability of successfully conducting the localization procedure and illustrates how this metric is influenced by various network parameters. Based on **Proposition 1**, the expected SINR is computed by: $\mathbb{E}\{\text{SINR}_k^{\text{PA}}\} = \int_0^\infty P(\text{SINR}_k^{\text{PA}} > \tau) d\tau$. Based on the expected SINR, the RSS disturbance σ_p^2 is obtained.

B. CRLB Analysis

Based on the RSS signal model given by (5), the Fisher information matrix (FIM) is given by

$$\text{FIM}_{\text{RSS}}(\mathbf{p}_t) = \frac{1}{\sigma_{\text{RSS}}^2} \begin{bmatrix} A & C \\ C & B \end{bmatrix}, \quad (9)$$

$$\begin{aligned} A &= \sum_{k=1}^K \frac{(x_{k,1} - x_t)^2}{d_{k,1}^4}, \quad B = \sum_{k=1}^K \frac{(y_{k,1} - y_t)^2}{d_{k,1}^4}, \\ C &= \left(\sum_{k=1}^K \frac{(x_{k,1} - x_t)(y_{k,1} - y_t)}{d_{k,1}^4} \right)^2, \end{aligned} \quad (10)$$

where $\sigma_{\text{RSS}} = \frac{\sigma_p}{\alpha}$, and $x_t = y_t = 0$. Note that the following analysis remains valid even when the target is not located at the origin. The CRLB for RSS-based localization is then:

$$\text{CRLB}_{\text{RSS}}(\mathbf{p}_t) = \text{tr}(\text{FIM}_{\text{RSS}}^{-1}(\mathbf{p}_t)) = \sigma_{\text{RSS}}^2 \frac{A + B}{AB - C^2}. \quad (11)$$

where $\text{tr}(\cdot)$ is the trace operation. In addition to deriving the CRLB using only the RSS samples detected from the nearest PA on each waveguide, the PA can be activated at different timestamps at all predefined locations on the waveguide for localization. In this case, the variables A , B , and C , can then be updated as follows:

$$\begin{aligned} \bar{A} &= \sum_{k=1}^K \sum_{m=0}^{M-1} \frac{(x_{k,m} - x_t)^2}{d_{k,m}^4}, \quad \bar{B} = \sum_{k=1}^K \sum_{m=0}^{M-1} \frac{(y_{k,m} - y_t)^2}{d_{k,m}^4}, \\ \bar{C} &= \left(\sum_{k=1}^K \sum_{m=0}^{M-1} \frac{(x_{k,m} - x_t)(y_{k,m} - y_t)}{d_{k,m}^4} \right)^2, \end{aligned} \quad (12)$$

where M is the number of predefined locations on each waveguide. By substituting (12) into (11), the RSS-based CRLB, considering all predefined locations for PA activation, can be obtained. However, (11) involves the random variables $x_{k,m}$, $y_{k,m}$, and $d_{k,m}$, which makes it challenging to derive the distribution of the CRLB. Motivated by this challenge, we employ the concept of mutual information to derive a tractable approximation of the CRLB, as presented in the following.

Proposition 2. *By assuming that K waveguides are selected for localization, while each waveguide has M predefined PA positions. Given the RSS disturbance σ_p^2 , the RSS CRLB can be approximated by*

$$\text{CRLB}_{\text{RSS}}(\mathbf{p}_t) \approx \sigma_{\text{RSS}}^2 \frac{4}{M(K-1)} d_*^2, \quad (13)$$

where $d_* \in \{d_{k,m}\}_{k=1, m=0}^{K, M-1}$ is the selected distance between the target user and the PA activated at the m -th predefined location on the k -th waveguide. Considering a practical scenario in which only a single PA on the waveguides is activated for localization, we can set $M = 1$.

Proof. See Appendix II. \square

Compared to the lengthy and complex expression in (11), the approximate CRLB presented in **Proposition 2** provides a concise and analytically tractable expression that effectively captures the localization performance. This simplified form serves as a valuable tool for performance evaluation without relying on computationally intensive simulations. It shows that (13) is a function of distance d_* , while the CDF of d_* is given in (2). The conditional RSS-based CRLB distribution is

$$\begin{aligned} & P(\text{CRLB}_{\text{RSS}}(\mathbf{p}_t) \leq s | M, K, \sigma_p^2) \\ & = P(d_* \leq \sqrt{sM(K-1)/2\sigma_p^2} | M, K, \sigma_p^2). \end{aligned} \quad (14)$$

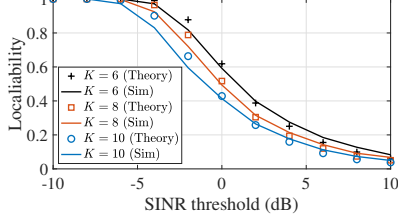


Fig. 2. Accuracy of **Proposition 1** versus different SINR thresholds.

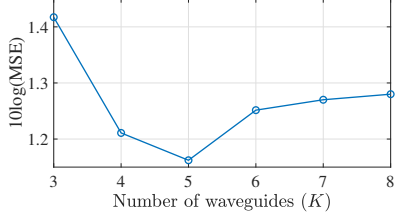


Fig. 3. The localization performance versus different numbers of waveguides.

By substituting the CDF of d_* into (14), the CRLB distribution for the PA system is obtained. Compared to conventional analytical methods that assume a fixed network geometry, the stochastic geometric framework accommodates random network deployments. By leveraging the inherent randomness of the considered PA system, the CRLB distribution provides insights into how the number of waveguides and channel parameters affect the overall localization performance across all possible geometric configurations.

Although this study considers RSS for localization, it was suggested in [4] that ToA measurements can be utilized for target localization. However, the time synchronization among the deployed waveguides cannot be overlooked during the localization process. To mitigate this impact, time-difference-of-arrival (TDoA) localization can be applied. In our previous work [15], the approximate CRLB for the TDoA-based localization is: $\text{CRLB}_{\text{TDoA}}(\mathbf{p}_t) \approx \frac{\sigma_{\tau}^2(K-1)}{\sum_{k=2}^K (1+\cos^2 \theta_k - 2 \cos \theta_k)}$, where θ_k is the angle from the nearest PA to the target on the k -th waveguide, while the range variance σ_{τ}^2 is computed by following [13]. The performance of the RSS-based method will be compared with that of using TDoA. For angle-based localization, estimating the AoA typically requires the use of antenna arrays [8], while a single PA or a target equipped with only a single antenna cannot extract angle information.

IV. NUMERICAL RESULTS

A. Simulation Setups

For the simulation setup, waveguides are modeled using a PLP with line density $\lambda_l = 0.1/\pi \text{ m}^{-1}$ in the 2-D disk with center point at the origin and radius $R_a = 30 \text{ m}$, while the pre-defined locations on each waveguide are randomly distributed according to a 1-D HPPP with density $\lambda_s = 0.1 \text{ m}^{-1}$. Each PA transmits signals with a constant power of $P_t = 1 \text{ W}$, and the path-loss exponent is set to $\alpha = 2.1$ [9]. All simulation results are averaged over 10^5 independent runs.

B. Tradeoff between Localizability and CRLB

Figure 2 illustrates the localizability performance of PA systems versus different SINR values. It is observed that

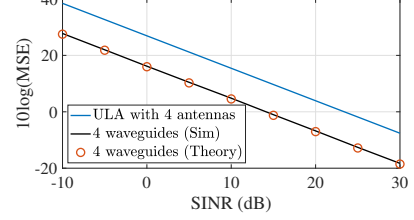


Fig. 4. Accuracy of **Proposition 2** versus different SINR values.

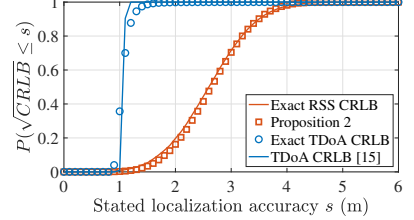


Fig. 5. Accuracy of CRLB distribution versus localization requirements.

localizability decreases as the required SINR increases. Although a higher SINR value guarantees better RSS quality, it is crucial to optimize network design to mitigate the impact of interference on localization performance. As the number of available waveguides increases, the overall localizability deteriorates. It is understandable that when different PAs transmit distinct pilots to the target for extracting RSS samples, an increase in the number of PAs results in greater interference.

Figure 3 provides insights into how the number of available waveguides K affects the overall localization performance. It is evident that increasing the number of waveguides does not always guarantee improved localization accuracy. When the number of available waveguides is limited (e.g., $K = 3$ to 5), the localization performance improves with K since the benefit of additional measurements outweighs the effect of interference. Notably, when $K = 5$, the RSS-based scheme achieves the lowest mean-square error (MSE), indicating the best localization performance. However, further increasing the number of waveguides results in worse localization performance, as interference becomes the dominant factor. Therefore, it is essential to determine the optimal number of waveguides for localization to balance the trade-off between interference and localization accuracy.

C. Overall Localization Performance

Figure 4 examines the performance of the RSS-based localization across different SINR values. The theoretical results generated by **Proposition 2** are consistent with the exact RSS-based CRLB obtained from (11). Furthermore, we compare PA system-assisted localization with conventional ULA-based localization. By adjusting the PA locations, the LoS distance between the PA and the target user is shortened, resulting in the acquisition of higher-quality RSS samples. The PA system also provides greater spatial diversity, whereas the ULA offers location-related measurement observations from only a single standpoint. Thus, the PA system systematically achieves better localization performance than the ULA.

Figure 5 shows that the theoretical results generated by (14) closely match the simulation results, verifying the the-

oretical development of the CRLB distribution. Compared to the exact CRLB (11), the CRLB distribution provides insights into the overall localization performance. For instance, Fig. 5 shows that the RSS-based scheme achieves 3-meter localization accuracy with a probability of 40%. We also compare the RSS-based scheme with the TDoA-based method [15]. Since RSS measurements are less stable in signal propagation environments, while high-resolution TDoAs can be leveraged for localization, the TDoA-based scheme in PA systems outperforms that of using RSS. However, in practice, obtaining accurate time measurements in a PA system without the assistance of additional receivers, such as a ULA or LCC, remains an open challenge. Thus, the RSS-based localization scheme remains a favorable solution for PA systems.

V. CONCLUSION

This paper presented a unified analytical framework for PA-assisted localization using stochastic geometry, modeling waveguides via a PLP. Our framework enables network-level performance analysis without intensive simulations and provides insights into selecting the optimal number of waveguides to achieve the optimal localization performance in terms of target localizability and CRLB. Numerical results showed that the PA-assisted system outperforms fixed-antenna systems, underscoring the benefits of using PAs for accurate positioning.

APPENDIX I

When $\alpha > 2$, given distances $d_{1,1}$, $d_{K,1}$, and ρ_k , the probability of detecting K waveguides is computed by

$$\begin{aligned} & P(\text{SINR}_K^{\text{PA}} > \tau | d_{1,1}, d_{K,1}, \rho_K) \\ & \approx F_{d_{K,1} | \rho_K} \left(\left[\tau (\mathbb{E}\{I\} + \sigma_n^2) \right]^{-\frac{1}{\alpha}} \right), \end{aligned} \quad (15)$$

while the interference from the remaining $K-2$ PAs (excluding the PA on the nearest waveguide to the target) is

$$\begin{aligned} & \mathbb{E} \left\{ \sum_{i=2}^{K-1} d_{i,1}^{-\alpha} \mid d_{1,1}, d_{K,1}, \rho_1, \rho_K \right\} \\ & = \sum_{i=2}^{K-1} \int_{d_{1,1}}^{d_{i+1,1}} r^{-\alpha} f_{d_{i,1} | \rho_i}(r) f_{\rho_i}(x) dr dx \\ & \stackrel{(a)}{\approx} \int_{\rho_1}^{\rho_K} \frac{2(K-2)r^{1-\alpha}}{\rho_K^2 - \rho_1^2} dr = \frac{2(K-2)}{2-\alpha} \frac{\rho_K^{2-\alpha} - \rho_1^{2-\alpha}}{\rho_K^2 - \rho_1^2}, \end{aligned} \quad (16)$$

where (a) simplifies the interference computation from $K-2$ PAs by considering that the nearest path between the target and the activated PA on the waveguide is the perpendicular distance ρ_k instead of $d_{k,1}$. Since the location on the waveguide associated with ρ_k follows a 2-D HPPP, the PDF of ρ_k is: $f_{\rho_k}(r) = \frac{2r}{\rho_K^2 - \rho_1^2}$. By substituting $f_{\rho_k}(x)$ into (16), the final expression is obtained. Based on a similar idea, the interference outside the circular $\mathbf{b}(O, \rho_K)$ is: $\mathbb{E}\{\sum_{i=K+1}^{\infty} d_{i,1}^{-\alpha}\} = 2\pi\lambda_l \int_{\rho_K}^{\infty} r^{-\alpha+1} dr = \frac{2\pi\lambda_l}{\alpha-2} \rho_K^{2-\alpha}$. For the case of $\alpha = 2$, the result can be derived in a similar manner.

APPENDIX II

Let the denominator of the RSS-based CRLB in (11) be $D = \bar{A}\bar{B} - \bar{C}^2$. We aim to select a distance $d_* = d_{p,q} \in \{d_{k,m}\}_{k=1, m=0}^{K, M-1}$ that provides the highest amount of information to D by maximizing the mutual information, which

is: $I(D; d_{k,m} | M, K) = h(D|M, K) - h(D|d_{k,m}, M, K)$, whereas the differential entropies are given by

$$\begin{aligned} h(D|M, K) &= - \int_{\bar{I}_D} f_D(D|M, K) \\ &\quad \times \log_2 f_D(D|M, K) dD, \\ h(D|d_{k,m}, M, K) &= - \int_{\bar{I}_D} \int_{\bar{D}} f_{D;d_{k,m}}(D, d_{k,m} | M, K) \\ &\quad \times \log_2 f_D(D|d_{k,m}, M, K) dD dd_{k,m}, \end{aligned} \quad (17)$$

where $f_D(\cdot)$ and $f_{D;d_{k,m}}(\cdot)$ are the PDFs of D and the joint PDF of D and $d_{k,m}$, respectively, while \bar{I}_D and \bar{D} denote the supports of D and $d_{k,m}$. These PDFs can be obtained through Monte-Carlo simulations. Based on the selected q -th PA on the waveguides, we have

$$\begin{aligned} \bar{A} &\approx M \sum_{k=1}^K \frac{(x_{k,q} - x_t)^2}{d_{k,q}^4}, \quad \bar{B} \approx M \sum_{k=1}^K \frac{(y_{k,q} - y_t)^2}{d_{k,q}^4}, \\ \bar{C} &\stackrel{(a)}{\approx} M^2 \sum_{k=1}^K \frac{(x_{k,q} - x_t)^2 (y_{k,q} - y_t)^2}{d_{k,q}^8}, \end{aligned} \quad (18)$$

where (a) follows Sedrakyan's inequality. By selecting the p -th waveguide based on mutual information, it yields

$$b \approx M \sum_{k=1}^K \frac{1}{d_{k,q}^2} \approx \frac{MK}{d_{p,q}^2}, \quad D \stackrel{(b)}{\approx} M^2 K(K-1)/4d_{p,q}^4, \quad (19)$$

where (b) applies [14, Proposition 1]. By substituting (19) into (11), the proof is completed.

REFERENCES

- [1] Z. Ding *et al.*, "Flexible-antenna systems: A pinching-antenna perspective," *IEEE Trans. Commun.*, 2025, early access.
- [2] A. Fukuda *et al.*, "Pinching antenna - using a dielectric waveguide as an antenna," *NTT DOCOMO Technical J.*, vol. 23, no. 3, pp. 5–12, Jan. 2022.
- [3] Z. Ding and H. V. Poor, "LoS blockage in pinching-antenna systems: Curse or blessing?," *IEEE Wireless Commun. Lett.*, vol. 14, no. 9, pp. 2798–2802, Sept. 2025.
- [4] Z. Ding, "Pinching-antenna assisted ISAC: A CRLB perspective," 2025, arXiv: <https://arxiv.org/abs/2504.05792>.
- [5] A. Khalili *et al.*, "Pinching antenna-enabled ISAC systems: Exploiting look-angle dependence of RCS for target diversity," 2025, arXiv: <https://arxiv.org/abs/2505.01777>.
- [6] Y. Qin *et al.*, "Joint antenna position and transmit power optimization for pinching antenna-assisted ISAC systems," *IEEE Wireless Commun. Lett.*, 2025, early access.
- [7] C. Ouyang *et al.*, "ISAC rate region of pinching-antenna systems," in *Proc. IEEE ICC*, Sep. 2025.
- [8] G. Zhou *et al.*, "Channel estimation for mmWave pinching-antenna systems," in *Proc. IEEE SPAWC*, pp. 1–5, Jul. 2025.
- [9] Z. Wang *et al.*, "Wireless sensing via pinching-antenna systems," *IEEE Wireless Commun. Lett.*, 2025, early access.
- [10] H. C. So and L. Lin, "Linear least squares approach for accurate received signal strength based source localization," *IEEE Trans. Signal Processing*, vol. 59, no. 8, pp. 4035–4040, May 2011.
- [11] D. Stoyan *et al.*, *Stochastic Geometry and its Applications*. John Wiley & Sons, 2013.
- [12] Y. Sun *et al.*, "Performance of downlink NOMA in vehicular communication networks: An analysis based on Poisson Line Cox point process," *IEEE Trans. Veh. Technol.*, vol. 69, no. 11, pp. 14001–14006, Sep. 2020.
- [13] H. C. So, *Source Localization: Algorithms and Analysis*. Ch. 3, pp. 59–106, John Wiley & Sons, Ltd, 2019.
- [14] J. He, Y. J. Chun, and H. C. So, "A unified analytical framework for RSS-based localization systems," *IEEE Internet Things J.*, vol. 9, no. 9, pp. 6506–6519, May 2022.
- [15] J. He *et al.*, "Modeling and performance analysis of blockchain-aided secure TDOA localization under random internet-of-vehicle networks," *Signal Processing*, vol. 206, p. 108904, Dec. 2022.